Transcriptional circuitry of NKX2-1 and SOX1 defines an unrecognized lineage subtype of small cell lung cancer

Ranran Kong[1,2,3], Ayushi S. Patel[2,3,4], Takashi Sato[2,3,5], Seungyeul Yoo[6,7], Li Bao[8], Abhilasha Sinha[2,3], Feng Jiang[2,3], Yang Tian[2,3], Maya Fridrikh[2,3], Shuhui Liu[9], Jie Feng[10], Xijing He[11,12], Jiantao Jiang[1], Yuefeng Ma[1], Karina Grullon[2,3], Dawei Yang[2,3,13], Charles A. Powell[2,3], Mary Beth Beasley[14], Jun Zhu[3,6,7], Eric L. Snyder[15,16], Shaomin Li[1]*, and Hideo Watanabe[2,3,6]*

[1]Department of Thoracic Surgery, The Second Affiliated Hospital of Medical School, Xi'an Jiaotong University, Xi'an, Shaanxi, 710004, China;

[2]Division of Pulmonary, Critical Care and Sleep Medicine, Department of Medicine, Icahn School of Medicine at Mount Sinai, New York, NY 10029, USA;

[3]Tisch Cancer Institute, Icahn School of Medicine at Mount Sinai, New York, NY 10029, USA;

[4]Division of Hematology & Medical Oncology, Laura and Isaac Perlmutter Cancer Center, New York University Langone Medical Center, New York, NY, USA;

[5]Department of Respiratory Medicine, Kitasato University School of Medicine, Sagamihara, Japan; Division of Pulmonary Medicine, Department of Medicine, Keio University School of Medicine, Tokyo, Japan;

[6]Department of Genetics and Genomic Sciences, Icahn School of Medicine at Mount Sinai, New York, NY 10029, USA;

[7]Sema4, a Mount Sinai venture, Stamford, CT 06902, USA;

[8]Ningxia People's Hospital, Yinchuan, Ningxia Province, 750001, China;

[9]Division of Infectious Diseases, Department of Medicine, Icahn School of Medicine at Mount Sinai, New York, NY 10029, USA;

[10]Department of Nephrology, The First Affiliated Hospital of Medical School, Xi'an Jiaotong University, Xi'an, Shaanxi, 710061, China;

26 [11]Department of Orthopedics, The Second Affiliated Hospital of Medical School, Xi'an Jiaotong University,
27 Xi'an, Shaanxi, 710004, China;
28 [12]Xi'an International Medical Center, Xi'an, Shaanxi, 710126, China;
29 [13]Department of Pulmonary and Critical Care Medicine, Zhongshan Hospital Fudan University, Shanghai,
30 200032, China;
31 [14]Department of Pathology and Laboratory Medicine, Icahn School of Medicine at Mount Sinai, New York,
32 NY 10029, USA;
33 [15]Department of Pathology, University of Utah, Salt Lake City, UT 84112; Department of Oncological
34 Sciences, University of Utah, Salt Lake City, UT 84112, USA;
35 [16]Huntsman Cancer Institute, University of Utah, Salt Lake City, UT 84112
36
37 * Both authors share senior authorship.
38

39 H.W. has been supported by ATS Foundation Unrestricted Grant (ATS-2017-24), the American
40 Lung Association of the Northeast Lung Cancer Discovery Award (LCD-504985), Department of
41 Defense (W81XWH-19-1-0613) and NIH (R01CA240342). R.K. is supported by Shaanxi
42 Provincial Natural Science Foundation, China (2017JM8046). T. S. is supported by the Japanese
43 Respiratory Society the 6th Lilly Oncology Fellowship Program and the Uehara Memorial
44 Foundation. J. F. is supported by National Natural Science Foundation of China (NSFC) (No.
45 82100718). D. Y. is supported by Shanghai Pujiang Program (20PJ1402400). C.A.P. and H. W.
46 are supported by NIH (R01CA163772). E.L.S. is supported by the NIH (R01CA212415,
47 R01CA240317) and the American Lung Association Lung Cancer Discovery Award (LCD-
48 821670). This work was supported in part through the computational resources and staff expertise
49 provided by Scientific Computing at the Icahn School of Medicine at Mount Sinai.

Correspondence and requests for reprints should be addressed to Hideo Watanabe, Division of Pulmonary, Critical Care and Sleep Medicine, Department of Medicine, Icahn School of Medicine at Mount Sinai, New York, NY 10029, USA. Phone: 212-241-9242; Fax: 212-876-5519; Email: hideo.watanabe@mssm.edu.

Author contributions: Conceptualization & Methodology, R.K., and H.W.; Data Collection: R.K., A.S.P., T.S., S.Y., L.B., F.J., M.F., S.L., J.F., X.H., J.J., Y.M., K.G., D.Y., E.L.S., S.L., L.S., and H.W.; Resources, E.L.S., M.B.B., C.A.P., S.L., and H.W.; Data Analysis, R.K., S.Y., A.S.P., S.L., M.B.B., E.L.S., and H.W.; Writing – Original Draft, R.K., A.S.P. and H.W.; Writing-Review & Editing, R.K., A.S.P., E.L.S., and H.W.; Supervision, C.A.P., J.Z. S.L., and H.W.; Project Administration & Funding Acquisition, H.W.

Running title: Collaboration of NKX2-1 and SOX1 defines SCLC-Aα subtype

Descriptor number: 9.26 Lung Cancer: Cellular and Molecular Aspects

The total word count for the body of the manuscript: 3,554

This article has an online data supplement, which is accessible from this issue's table of content online at www.atsjournals.org

Abstract:

Rationale: The current molecular classification of small cell lung cancer (SCLC) based on expression of four lineage transcription factors still leaves its major subtype SCLC-A as a heterogeneous group, necessitating more precise characterization of lineage subclasses.

Objectives: To refine the current SCLC classification with epigenomic profiles and to identify features of the re-defined SCLC subtypes.

Methods: We performed unsupervised clustering of epigenomic profiles on 25 SCLC cell lines. Functional significance was evaluated by cell growth, apoptosis and xenograft using CRISPR-Cas9-mediated deletion. The specific cistromic profiles by ChIP-seq and its functional transcriptional partners using co-immunoprecipitation followed by mass spectrometry were determined. *Rb1*$^{fl/fl}$*Trp53*$^{fl/fl}$ and *Rb1*$^{fl/fl}$*Trp53*$^{fl/fl}$*Nkx2-1*$^{fl/fl}$ mouse models were engineered to explore the function of *Nkx2-1* in tumor initiation and differentiation. H3K27ac profiles were analyzed to reveal 6 human SCLC specimen and 20 mice tumors epigenomic landscapes.

Measurements and Main Results: We identified an epigenomic subclusters of the major SCLC-A subtype, named SCLC-Aα and SCLC-Aσ. SCLC-Aα was characterized by the presence of a super-enhancer at the *NKX2-1* locus, which was observed in human SCLC specimens and a murine SCLC model. We found NKX2-1, a dual lung and neural lineage factor, is uniquely relevant in SCLC-Aα. We further found maintenance of this neural identity in SCLC-Aα is mediated by collaborative transcriptional activity with another neuronal transcriptional factor SOX1.

Conclusions: We comprehensively describe an additional epigenomic heterogeneity of the major SCLC-A subtype, and define SCLC-Aα subtype by the core regulatory circuitry representing NKX2-1 and SOX1 super-enhancers and their functional collaborations to maintain neuronal linage state. (Word count 250)

93 **Keywords:** small cell lung cancer (SCLC); *NKX2-1/TTF-1*; *SOX1*; Super-enhancer

94 **INTRODUCTION**

95 Small cell lung cancer (SCLC) is an aggressive, lethal, and rapidly progressing neuroendocrine
96 (NE) malignancy, accounting for ~15% of lung cancer incidence and 250,000 deaths worldwide
97 annually (1). The five-year survival rate for patients with SCLC is only 6% compared to 19% for
98 non-SCLC. The lack of progress in SCLC treatment is largely attributable to the inadequate
99 molecular understanding. Advances in genomic technology have enabled new molecular
100 characterization of SCLCs. Genome-wide methylation and transcriptomes of human SCLCs and
101 PDX models identified NE and non-NE subtypes. NE subtype is defined by the expression of
102 neuronal lineage transcription factors (TFs) ASCL1 and/or NeuroD1 (2). Two recent studies
103 described the non-NE SCLCs, one signified by YAP1 expression and another by POU2F3
104 expression (3, 4). In light of these findings, a consortium proposed a new molecular classification
105 of SCLCs that distinguishes them into four subtypes based on the expression of four lineage-
106 defining transcription factors: ASCL1, NeuroD1, YAP1 and POU2F3 referred to as SCLC-A,
107 SCLC-N, SCLC-Y and SCLC-P, respectively (5, 6). The classification, while marking significant
108 advance, is still a work in progress. After that report, a newer study proposed an inflamed SCLC
109 subtype (SCLC-I) (7). In addition, not all SCLCs clearly fall into the four clusters as they often
110 express multiple factors at variable levels, especially in the SCLC-A subtype which account for
111 70% of SCLCs (8). This wide range of heterogeneity warrants novel approaches to develop a more
112 precise classification of SCLC based on lineage subtype.

113 Lineage-specific transcription factors and the presence of SE at their gene locus are critical
114 determinants of cellular identity (9). In our study, we applied epigenomic approaches to investigate
115 the differential enhancer landscapes in SCLC cell lines, human SCLC samples and autochthonous
116 murine SCLCs from a genetic engineered mouse model (GEMM) to reveal additional intertumoral

117 heterogeneity, providing comprehensive evidence of distinct histone modification profiles.
118 Furthermore, we determined a novel mechanism of subtype-specific transcriptional regulation in
119 SCLC, integrating the core transcriptional networks and their collaborative regulation of NE target
120 genes.

121 **METHODS**

122 For a detailed description of the methods, please see the online supplement.

123 ***Cell lines***

124 Cell lines used in this study are listed in Table E1.

125 ***Chromatin Immunoprecipitation followed by sequencing (ChIP-seq)***

126 ChIP-seq was performed as described previously (10). Protein G magnetic beads (Dynabeads: Life
127 Technologies) were pre-incubated with anti-H3K27ac (Abcam, ab4729) or anti-NKX2-1 (Bethyl
128 Laboratories, A300-BL4000) or anti-SOX1 (R&D, AF3369) antibodies. Up to 10 ng of DNA was
129 used for the library construction using NEBNext Ultra II DNA Library Prep Kit (NEB, E7645).
130 Sequencing was performed on NextSeq 500 (Illumina).

131 ***RNA-seq***

132 The procedure was performed as previously described (8, 10).

133 ***Lentiviral transduction of genes and CRISPR-Cas9 genome editing***

134 *FLAG-NKX2-1* or *FLAG-GFP* open reading frame (ORF) was cloned into pLEX_306 (a gift from
135 David Root, Addgene plasmid #41391). Cells stably expressing Cas9 were generated by infection
136 with the lentiCas9-Blast plasmid (Addgene # 52962, a gift from Feng Zhang). sgRNAs targeting
137 *NKX2-1* or *SOX1* were selected from Brunello library (Table E2) (11). Additional details are
138 provided in the online supplement.

139 ***Immunohistochemistry (IHC)***

140 Immunohistochemical analyses were performed on xenograft tumor specimens, human primary
141 SCLC tumor specimens and genetic engineered mouse model (GEMM) tumor specimens with
142 anti-NKX2-1 (1:100; Santa Cruz, sc-53136), anti-SOX1 (R&D, AF3369) or anti-ASCL1 (1:100,
143 BD, 556604) antibody and detected with the Vectastain ABC kit.

144 ***Co-immunoprecipitation and LC-MS/MS***

145 Chromatin fraction was prepared and co-immunoprecipitated with the methods described
146 previously (12) with modifications. Peptides were detected, isolated, and fragmented to produce a
147 tandem mass-spectrum of specific fragment ions for each peptide with LTQ Orbitrap Velos Pro
148 ion-trap mass spectrometer (Thermo Fisher Scientific, Waltham, MA).

149 ***Cell proliferation assay***

150 AlamarBlue Cell Viability Reagent was used to analyze cell proliferation. Cells were plated at a
151 density of 3,000 cells/well with five replicates in a 96-well plate.

152 ***Xenograft model***

153 The procedure was performed as previously described (ref). All xenograft studies were approved
154 by the institutional Animal Care and Use Committee at Icahn School of Medicine at Mount Sinai
155 (IACUC-2018-0021).

156 ***Annexin-V staining***

157 Alexa Fluor® 488 annexin V/Dead Cell Apoptosis Kit (Thermo Fisher Scientific) was used
158 according to manufacturers' recommendations. Fluorescence was measured by FACS Canto II
159 (BD Bioscience).

160 ***In situ proximity ligation assay (in situ PLA)***

161 *In situ* PLA was performed with DuoLink in Situ Reagents (Sigma) according to the instructions.
162 Images were acquired with a ZEISS Axiocam 503 mono confocal microscope.

163 ***Mice and tumor initiation***

164 Mice harboring $Rb1^{flox}$, $Trp53^{flox}$ and $Nkx2\text{-}1^{flox}$ alleles have been previously described (13, 14).
165 Tumors were generated by intratracheal delivery of Ad5CMV-Cre adenovirus (University of Iowa,
166 Gene Transfer Vector Core) as described (15). All studies were approved by the Committee for
167 Animal Care at MIT (A-3125–01).

168 ***Data analysis***

169 Details are provided in the online supplement.

170 ***Statistical Analysis***

171 Details of specific analyses are provided in the figure legends.

172 ***Data and materials availability***

173 SCLC cell lines, human primary SCLC tumors, RP and RPN tumors H3K27ac ChIP-seq, Cell lines
174 and RP and RPN tumors RNA-seq, NKX2-1 and SOX1 ChIP-seq are deposited in NCBI GEO:
175 GSE183373.

176 **RESULTS**

177 **Epigenomic profiling subdivided SCLC-A by differential super-enhancers**

178 Genome-scale chromatin organization of the cell more faithfully reflects their lineage state than
179 transcriptomics (16). To refine current SCLC classification, we profiled genome-wide H3K27ac
180 to define SE regions across 16 SCLC cell lines. Unsupervised hierarchical clustering on SEs on
181 genes for transcriptional regulation with additional public data (4) revealed four subclasses (Figure
182 1A), supported by principal component analysis (PCA) (see Figure E1A in the online data
183 supplement). Our clusters recapitulated aspects of the expression classification. Cluster III
184 corresponds to SCLC-N (Figure 1A; purple). Cluster IV represents SCLC-P and SCLC-Y (Figure
185 1A; blue). Notably, epigenomic clustering distinguished SCLC-A into two distinct Clusters I and
186 II (Figure 1A; red and green) referred to as SCLC-Aα and SCLC-Aσ, while *ASCL1* SE is present
187 in 92.9% (13/14) of SCLC-A (Figure E1B).

188 To understand the difference underpinning SCLC-Aα and SCLC-Aσ, we identified 140
189 differentially enriched SEs. Among 110 SEs enriched in SCLC-Aα was *NKX2-1* (Figure 1B),
190 where H3K27ac signal was largely absent in other subclasses (Figure 1C). The 30 SEs enriched in
191 SCLC-Aσ included *TCF4*, a transcription factor that regulates synaptic plasticity (17) (Figure 1B
192 and Figure E1B). NKX2-1, also known as *TTF1*, a lineage transcription factor essential for the
193 development and maintenance of lungs, brain, and thyroid, is a frequently amplified lineage-
194 specific oncogene and a well-known marker to diagnose lung adenocarcinoma (LADC) (18) (19,
195 20). However, *NKX2-1* is not significantly amplified in human SCLCs (21) nor in the SCLC lines
196 used (Figure E1C). Nonetheless, SCLC-Aα cell lines harbor *NKX2-1* SE, whereas SCLC-Aσ cell
197 lines do not (Figure 1D and Figure E1D). Local H3K27ac enrichment pattern at the *NKX2-1* locus
198 in SCLC-Aα was almost identical to LADCs with *NKX2-1* amplification (Figure E1E). In 6 human

199 SCLC specimens, we found one SCLC-P tumor with *POU2F3* SE, and threes mixed SCLC-A/N
200 tumors with SEs near *ASCL1* and *NEUROD1* loci (Figure E1F). Notably, we observed two tumors
201 representing SCLC-Aα with high signals at *ASCL1* and *NKX2-1* loci (Figure 1E).

202 By immunohistochemistry (IHC) on another 34 human SCLC cohort, 65% (22/34) of cases
203 were NKX2-1-positive (Figure E2A), consistent with prior studies (22-26). In cell lines, SCLC-
204 Aα expressed substantially higher levels of NKX2-1 protein than other SCLC subtypes and
205 equivalent to *NKX2-1*-amplified LADCs (Figure 1F). Furthermore, RNA-seq datasets (5, 27)
206 confirmed *NKX2-1* is highly expressed in SCLC (Figure E2B), particularly in SCLC-A (Figure
207 1G), comparable to the levels in LADC (Figure E2C), consistent with a previous report (22).
208 Nonetheless, non-bimodal distribution of *NKX2-1* expression suggests that the distinction between
209 SCLC-Aα and Aσ is not discernible from expression analysis, perhaps analogous to the findings
210 that *NKX2-1* is almost universally expressed in LADC yet only amplified in 10-15%, which we
211 previously characterized as a distinct biological subgroup (19, 28).

212 ***NKX2-1* survival dependency is unique to SCLC-Aα**

213 A recent study implicated that NKX2-1 promotes SCLC growth and regulates NE differentiation
214 and anti-apoptosis (29). We deleted *NKX2-1* in SCLC-Aα cell lines (Figure 2A) and found it
215 significantly suppressed cell growth and increased annexin-V-positive populations (Figure 2C and
216 E3A). By contrast, ablating NKX2-1 in SCLC cells from other clusters (Figure 2B) had little effect.
217 Given that acute removal of a master lineage factor in established cancer often leads to a halt in
218 cell growth (30), these data suggest NKX2-1 does not play a general oncogenic role in all lineage
219 states but its function is uniquely relevant to SCLC-Aα.

220 We further found a significant decrease in tumor volume for NKX2-1-deleted SCLC-Aα
221 cells in xenograft (Figure 2D and Figure E3B), confirming its essentiality *in vivo*. No obvious

222 histological differences were observed in the cells that formed small tumors which escaped from
223 NKX2-1 deletion (Figure E3C). In a short period after NKX2-1 deletion *in vitro*, expression of NE
224 markers was not significantly altered (Figure E3D). Overall, these data suggest that NKX2-1 is
225 functionally critical for SCLC-Aα *in vitro* and *in vivo*.

226 **Genomic occupancy of *NKX2-1* in SCLC-Aα cells distinct from that in LADC cells**

227 In LADC, NKX2-1 regulates gene expression and shares its cistromes with normal lung
228 (19); however, SCLCs typically do not express canonical NKX2-1 targets. Given NKX2-1's roles
229 in subsets of cortical, striatal, and pallidal neurons (31), we speculated its potential role for
230 neuronal differentiation in SCLC-Aα. Therefore, we profiled NKX2-1 cistromes by ChIP-seq in 5
231 SCLC-Aα cell lines and compared them to that from 3 LADC cell lines. Pairwise correlation
232 coefficient of all NKX2-1-bound sites and PCA revealed histology-specific binding profiles
233 (Figure 3A and E4A). Regions 4 (low-intensity signals) and 1 (high-intensity signals) are common
234 between SCLC-Aα and LADC (Figure 3B), which included the *RUNX1* locus (Figure 3C). Region
235 3 was unique to LADC that included *LMO3,* an essential mediator of NKX2-1 functions in LADCs
236 (19). Region 2 was unique to SCLC-Aα that included *DCC,* a receptor for netrin required for axon
237 guidance (32) (Figure 3C). These data suggest NKX2-1 regulates distinct transcriptional programs
238 across these two lineage states.

239 Ontologies on 661 SCLC-Aα-unique regions (Figure 3D and E4B) were enriched for
240 neuronal development, differentiation, and structure (Figure 3E). By contrast, genes regulating
241 neuronal biology were absent in LADC-unique regions (Figure E4C). Motif analysis revealed
242 SCLC-Aα-specific sites are enriched with ASCL2, Olig2, and SOX motifs, suggesting more
243 association with neuronal TFs (Figure E4D). In contrast, AP-1, Ets, Runx, and Tead-binding
244 motifs are enriched in LADC-specific regions, consistent with our previous report (19). These data

245 indicate that contribution of NKX2-1 in regulating pathways for maintenance of neural
246 differentiation state of SCLC-Aα, distinct from its role in normal lung epithelium and LADCs.

247 **NKX2-1 interactome in chromatin of SCLC-Aα cells includes SOX1**

248 NKX2-1 interacts with FOXA1 to co-regulate the expression of a set of genes for lineage control
249 in LADC (19, 20). Therefore, to identify unique partners that interact with NKX2-1 to exert distinct
250 transcriptional program in SCLC-Aα, we performed co-immunoprecipitation (co-IP) followed by
251 liquid chromatography tandem mass-spectrometry (LC-MS/MS) in the chromatin fraction of two
252 SCLC-Aα cell lines ectopically expressing FLAG-NKX2-1 (Figure 4A and Figure E5A). We
253 found 27 overlapping NKX2-1-interacting TFs in both cell lines (Figure 4B).

254 We further identified core regulatory circuitries (CRCs) (33) for SCLC-Aα and other SCLC
255 clusters from our H3K27ac data. Common CRCs included NEUROD1 for SCLC-N, POU2F3 and
256 ASCL2 for SCLC-P/Y, and TCF4 in SCLC-Aσ, consistent with our differential SE analysis
257 (Figure 1B and E5B). Common CRCs in SCLC-Aα included NKX2-1 (Figure 4C) along with
258 SOX1, NFIB, TCF12 and PBX1 also found in the SCLC-Aα NKX2-1-interactome. Of those,
259 H3K27ac signal at *SOX1* was highly enriched in SCLC-Aα (Figure 1B and Figure 4D), whereas
260 *NFIB*, *TCF12* and *PBX1* SEs were present across SCLC subtypes (Figure E5C). *SOX1* is highly
261 expressed in SCLC-A (Figure E5D) and positively correlated with *NKX2-1* expression in 185
262 SCLC tumors and cell lines (Figure E5E). SOX1 protein was also highly expressed specifically in
263 SCLC-Aα cell lines (Figure E5F).

264 The interaction between NKX2-1 and SOX1 was confirmed by co-IP followed by western
265 blot in two SCLC-Aα cell lines (Figure 4E), and further by proximity ligation assay (PLA) in 4
266 SCLC-Aα cell lines (Figure 4F and Figure E5G). These data suggest robust protein-protein
267 interaction between NKX2-1 and SOX1 uniquely in SCLC-Aα.

268 **NKX2-1 and SOX1 co-occupy the SCLC-Aα genome to collaborate in neuronal gene**
269 **regulation**

270 Next, we profiled genome-wide binding profiles of NKX2-1 and SOX1 in four SCLC-Aα cell lines
271 and found the majority of SOX1 peaks were bound by NKX2-1 (48.6-67.8%) (Figure 5A). The
272 2,652 regions co-bound by NKX2-1 and SOX1 in NCI-H187 were enriched for functions in neuron
273 differentiation and development, consistent with the aggregate analysis (Figure E6A and E6B).
274 We defined high-confidence NKX2-1 (5,663) and SOX1 (1,101) binding sites observed in ≧3 cell
275 lines, and found 604 peaks (54.9% of SOX1 peaks) are overlapped (Figure 5B), which included
276 the *NKX2-1* locus as well as neuronal genes *NRXN3* (34, 35) and *YWHAZ* (36) (Figure 5C) and
277 ontologically enriched for functions in neuron differentiation and development (Figure 5D). These
278 data suggest the interaction between NKX2-1 and SOX1 elicits specific cellular identity of SCLC-
279 Aα.

280 **Collaboration of NKX2-1 and SOX1 is required to control the neuronal state in SCLC-Aα**

281 We evaluated the transcriptional effect of depletion of *SOX1* or *NKX2-1* in NCI-H187 by RNA-
282 seq. After the abrogation of NKX2-1 or SOX1, 1,121 and 2,499 genes were significantly
283 downregulated respectively, with 873 genes commonly downregulated, suggesting a substantial
284 overlap in their transcriptional outputs (Figure 6A). We then queried the differentially co-
285 downregulated genes with the 2,652 genes with transcriptional start sites (TSSs) within 50 kb of
286 SOX1-NKX2-1 co-occupied peaks in NCI-H187, which were significantly enriched for NKX2-1
287 or SOX1 downregulated genes by ssGSEA analysis (Figure 6B). Leading edge analysis on these
288 genes revealed 289 overlaps, which we found are enriched for neuron differentiation and
289 development (Figure 6C). Together, these data suggest that NKX2-1 and SOX1 are specifically
290 co-localized on the SCLC-Aα genome and collaboratively contribute to controlling neuronal

291 differentiation state. We also found that SOX1 deletion, while not affecting the NKX2-1
292 expression, led to reduced cell growth (Figure E7A) with increased apoptosis (Figure E7B).
293 We previously found that expression of Nkx2-1 was critical for global Foxa1/2 binding
294 pattern in the LADC genome (20). To test if SOX1 is required for NKX2-1-binding to its target
295 genes in SCLC-Aα, we performed NKX2-1 ChIP-seq in NCI-H187 cells upon SOX1 depletion.
296 Pairwise correlation coefficient of NKX2-1 peaks across cells deleted for SOX1 or control
297 revealed strong correlation amongst each group (Figure 6D), supported by PCA analysis (Figure
298 E7C). Differential analysis on NKX2-1-bound sites found 2,067 peaks decreased upon SOX1
299 deletion (Figure E7D). *k*-means clustering of the differential sites found relatively uniform
300 reduction of NKX2-1 binding after SOX1 deletion (Figure 6E), where we also found decreased
301 H3K27ac modification compared to other sites (Figure 6F), suggesting that these NKX2-1-lost
302 sites are no longer in active state, similar to a recent finding on Sox2 in esophageal squamous cell
303 cancer model for Klf5 (37). The data suggest that loss of SOX1 releases NKX2-1 from co-occupied
304 loci in SCLC-Aα.

305 ***Nkx2-1* is essential for development of SCLC-Aα tumors in an autochthonous mouse model**

306 The *Rb1*$^{fl/fl}$*Trp53*$^{fl/fl}$ (RP) is commonly used SCLC models that recapitulates the biology of
307 ASCL1-positive/classic human SCLCs (13) (Figure 7A). We first profiled H3K27ac to identify
308 SEs in mSCLC tumors from RP model, where Nkx2-1 is diffusely expressed. We found all 10
309 tumors from 2 different mice harbored high-level H3K27ac signal around the *Ascl1* locus, but none
310 harbored SEs at the *Neurod1*, *Yap1* or *Pou2f3* locus, suggesting SCLC-A subtype (Figure 7B and
311 Figure E8A) consistent with requirement of *Ascl1* for tumor formation in this model (38, 39). We
312 found 3 of 10 tumors simultaneously had high-level H3K27ac signals at the *Nkx2-1* and *Sox1* loci,
313 reminiscent of SCLC-Aα, while other 7 tumors have neither. This suggests that RP can adopt an

314 epigenetic state resembling either SCLC-Aα or SCLC-Aσ. Consistent but ambiguous expression
315 levels by IHC suggested epigenetic profiles distinguish these lineage classes more clearly (Figure
316 7C).

317 To explore whether NKX2-1 contributes to mSCLC differentiation, we generated
318 *Rb1*$^{fl/fl}$*Trp53*$^{fl/fl}$*Nkx2-1*$^{fl/fl}$ (RPN) mice. We confirmed Nkx2-1 expression was absent in their tumors,
319 while 80% of them are Ascl1-positive suggesting that they remain representing SCLC-A. Sox1
320 staining was only weakly positive in 6/10 cases while 4 other cases, including the two Ascl1-
321 negative tumors, were negative (Figure 7C). We observed no significant difference in overall
322 survival between the two genotypes (Figure E8B). Morphologically, all but one mSCLC tumor
323 from the RP model had classical SCLC morphology (scant cytoplasm, nuclei with fine chromatin
324 and inconspicuous nucleoli), whereas a subset of tumors in RPN mice (15% in RPN vs. 4% in RP)
325 exhibited a 'non-classical' histology defined by higher grade/vesicular nuclei by two expert
326 pathologists (E.L.S. and M.B) (Figure 7D). These suggest that loss of *Nkx2*-1 leads to stochastic
327 propensity to form non-classical morphology, the while majority of the tumors retain classical
328 histology representing SCLC-A.

329 Next, we profiled H3K27ac in 10 mSCLC tumors from four RPN mice (11-13 months
330 post-initiation, including five classical and five non-classical). None of the tumors from the RPN
331 mice had high-level H3K27ac signal at the *Neurod1*, *Yap1* or *Pou2f3* loci, whereas most of RPN
332 tumors (7/10) harbored high-level H3K27ac signals around the *Ascl1* locus (Figure 7B and Figure
333 E8A). Strikingly, we found signals at the *Nkx2-1* and the *Sox1* loci were absent in all RPN tumors,
334 suggesting SCLC-Aσ subtype (Figure 7B). These data suggest that while the RP model can
335 develop both SCLC-Aα and SCLC-Aσ, *Nkx2-1* deletion at tumor initiation precludes SCLC-Aα
336 development.

337 Differential transcriptomic analysis from the tumors in RPN and RP mice also revealed
338 significantly downregulated genes in RPN tumors enriched for nervous system development
339 (Figure 7E), suggesting that SCLC-Aσ is hierarchically closer to the SCLC-N and SCLC-Y/P
340 subtypes, also supported by the data that variant morphology is more frequent in RPN. To address
341 whether the absence of Nkx2-1 resulted in distinct tumor evolution in RPN, we profiled copy
342 numbers of those mSCLCs and found that *Nfib* and *Mycl* loci are frequently amplified in RP model
343 (6/10) consistent with previous reports; however, these amplifications were absent in all tumors in
344 RPN model, suggesting the lack of Nkx2-1 predisposed those RPN tumors to undergo a distinct
345 path leading to a different lineage class of tumors (Figure 7F and Figure E8C).

346 **DISCUSSION**

347 In the current classification, SCLC-A constitutes 70% of SCLCs, while emerging evidence
348 suggests its heterogeneity. Our study revealed distinctive epigenetic landscapes within SCLC-A
349 that we designated SCLC-Aα and SCLC-Aσ, characterized by the presence of *NKX2-1* and *TCF4*
350 SEs. NKX2-1 is required for the lung development and later specification of the peripheral lung,
351 but also of bronchial NE cells (40). NKX2-1 is a well-known marker to diagnose LADCs (41), but
352 it is also frequently expressed in SCLC. As NKX2-1 plays key roles in brain development (42-45),
353 it has been speculated that NKX2-1 is involved in NE pathways, based on its expression enriched
354 in SCLC-A (46) and its physical interaction with ASCL1 (29). In our study, while most SCLC-A
355 expresses NKX2-1 at variable levels, only 48% had *NKX2-1* SE. Importantly, *NKX2-1* deletion in
356 SCLC-Aσ and SCLC-N cells, where NKX2-1 protein is still expressed, had little cell growth
357 effects, suggesting its relevancy only in SCLC-Aα.

358 Further, our data suggest this function is mediated through interaction with SOX1.
359 Combinations of master TFs that assemble at tissue-specific cis-regulatory sites control distinct

360 cellular functions essential for maintaining lineage states in many contexts. Therefore, while the
361 role of SOX1 had never been described in the lung, it is plausible that their interaction is critical
362 to retain unique NE state and it further suggests biological plasticity between glandular cell lineage
363 and pulmonary NE lineage.

364 The roles of NKX2-1 in carcinogenesis are complex and remain poorly understood. Nkx2-
365 1 deletion in neoplastic lungs causes loss of pulmonary identity and reversion to a foregut lineage.
366 Our data suggest that Nkx2-1 contributes to maintaining a specific neural lineage state that have
367 classical SCLC morphology. The observation that *Nkx2-1* deletion is tolerated at tumor initiation
368 in the GEMM, but not in established human SCLC-Aα cell lines, provokes a few potential
369 interpretations. First, the timing of the deletion might be critical in determining the outcome, as
370 evidenced in other studies on lineage factors (47, 48). Second, as CMV-Cre targets multiple cell
371 types, *Nkx2-1* deletion may favor origination from certain cell types, thus influencing tumor
372 evolution, as reflected by the lack of amplification at *Nfib* and *Mycl*. Third, early/in situ RPN
373 lesions that would have become SCLC-Aα might simply evolve to an alternative identity due to
374 lack of *Nkx2-1*.

375 Together, we subdivided the major SCLC-A subtype into SCLC-Aα and SCLC-Aσ by
376 revealing distinct epigenetic landscape in SCLC cell lines, human SCLC tumors, and GEMM.
377 Collaborative NKX2-1/SOX1 regulation defines the unique lineage state for SCLC-Aα. This study
378 will provide foundation for future identification of vulnerabilities and enable us to develop higher
379 level of personalized therapeutic approaches to benefit SCLC patients.

Acknowledgements

We thank Hong Cai, Yi Ge, Ying Liu, Peipei Guo, Yifei Sun, Xiaokun Liu, Korey Kam, Mingzhe Li, Megan Vetter, Tyler Jacks and Karen Yee for helpful discussions and technical assistance, Aleksandra Wroblewska and Brian D. Brown for providing a lentiviral vector for cloning sgRNAs; NextSeq Sequencing Facility of the Department of Oncological Sciences at Icahn School of Medicine at Mount Sinai (ISMMS), Saboor Hekmaty, Gayatri Panda and Ravi Sachidanandam for sequencing assistance. The authors also thank Taplin Mass Spectrometry Facility at Harvard Medical School, the Biorepository and Pathology Core Facility at ISMMS and Center for Comparative Medicine and Surgery at the Icahn School of Medicine at Mount Sinai. Graphical Abstract was created with BioRender.com.

390 **References**

391 1. Siegel RL, Miller KD, Jemal A. Cancer statistics, 2019. *CA Cancer J Clin* 2019; 69: 7-34.
392 2. Poirier JT, Gardner EE, Connis N, Moreira AL, de Stanchina E, Hann CL, Rudin CM. DNA methylation in
393 small cell lung cancer defines distinct disease subtypes and correlates with high expression of
394 EZH2. *Oncogene* 2015; 34: 5869-5878.
395 3. McColl K, Wildey G, Sakre N, Lipka MB, Behtaj M, Kresak A, Chen Y, Yang M, Velcheti V, Fu P, Dowlati A.
396 Reciprocal expression of INSM1 and YAP1 defines subgroups in small cell lung cancer. *Oncotarget*
397 2017; 8: 73745-73756.
398 4. Huang YH, Klingbeil O, He XY, Wu XLS, Arun G, Lu B, Somerville TDD, Milazzo JP, Wilkinson JE, Demerdash
399 OE, Spector DL, Egeblad M, Shi JW, Vakoc CR. POU2F3 is a master regulator of a tuft cell-like
400 variant of small cell lung cancer. *Gene Dev* 2018; 32: 915-928.
401 5. George J, Lim JS, Jang SJ, Cun Y, Ozretic L, Kong G, Leenders F, Lu X, Fernandez-Cuesta L, Bosco G, Muller
402 C, Dahmen I, Jahchan NS, Park KS, Yang D, Karnezis AN, Vaka D, Torres A, Wang MS, Korbel JO,
403 Menon R, Chun SM, Kim D, Wilkerson M, Hayes N, Engelmann D, Putzer B, Bos M, Michels S, Vlasic
404 I, Seidel D, Pinther B, Schaub P, Becker C, Altmuller J, Yokota J, Kohno T, Iwakawa R, Tsuta K,
405 Noguchi M, Muley T, Hoffmann H, Schnabel PA, Petersen I, Chen Y, Soltermann A, Tischler V, Choi
406 CM, Kim YH, Massion PP, Zou Y, Jovanovic D, Kontic M, Wright GM, Russell PA, Solomon B, Koch
407 I, Lindner M, Muscarella LA, la Torre A, Field JK, Jakopovic M, Knezevic J, Castanos-Velez E, Roz L,
408 Pastorino U, Brustugun OT, Lund-Iversen M, Thunnissen E, Kohler J, Schuler M, Botling J, Sandelin
409 M, Sanchez-Cespedes M, Salvesen HB, Achter V, Lang U, Bogus M, Schneider PM, Zander T, Ansen
410 S, Hallek M, Wolf J, Vingron M, Yatabe Y, Travis WD, Nurnberg P, Reinhardt C, Perner S, Heukamp
411 L, Buttner R, Haas SA, Brambilla E, Peifer M, Sage J, Thomas RK. Comprehensive genomic profiles
412 of small cell lung cancer. *Nature* 2015; 524: 47-53.
413 6. Rudin CM, Poirier JT, Byers LA, Dive C, Dowlati A, George J, Heymach JV, Johnson JE, Lehman JM,
414 MacPherson D, Massion PP, Minna JD, Oliver TG, Quaranta V, Sage J, Thomas RK, Vakoc CR, Gazdar
415 AF. Molecular subtypes of small cell lung cancer: a synthesis of human and mouse model data.
416 *Nat Rev Cancer* 2019; 19: 289-297.
417 7. Gay CM, Stewart CA, Park EM, Diao L, Groves SM, Heeke S, Nabet BY, Fujimoto J, Solis LM, Lu W, Xi Y,
418 Cardnell RJ, Wang Q, Fabbri G, Cargill KR, Vokes NI, Ramkumar K, Zhang B, Della Corte CM, Robson
419 P, Swisher SG, Roth JA, Glisson BS, Shames DS, Wistuba, II, Wang J, Quaranta V, Minna J, Heymach
420 JV, Byers LA. Patterns of transcription factor programs and immune pathway activation define
421 four major subtypes of SCLC with distinct therapeutic vulnerabilities. *Cancer Cell* 2021; 39: 346-
422 360 e347.
423 8. Patel AS, Yoo S, Kong R, Sato T, Sinha A, Karam S, Bao L, Fridrikh M, Emoto K, Nudelman G, Powell CA,
424 Beasley MB, Zhu J, Watanabe H. Prototypical oncogene family Myc defines unappreciated distinct
425 lineage states of small cell lung cancer. *Sci Adv* 2021; 7.
426 9. Iwafuchi-Doi M, Zaret KS. Pioneer transcription factors in cell reprogramming. *Genes Dev* 2014; 28:
427 2679-2692.
428 10. Sato T, Yoo S, Kong R, Sinha A, Chandramani-Shivalingappa P, Patel A, Fridrikh M, Nagano O, Masuko
429 T, Beasley MB, Powell CA, Zhu J, Watanabe H. Epigenomic profiling discovers trans-lineage SOX2
430 partnerships driving tumor heterogeneity in lung squamous cell carcinoma. *Cancer Res* 2019.
431 11. Doench JG, Fusi N, Sullender M, Hegde M, Vaimberg EW, Donovan KF, Smith I, Tothova Z, Wilen C,
432 Orchard R, Virgin HW, Listgarten J, Root DE. Optimized sgRNA design to maximize activity and
433 minimize off-target effects of CRISPR-Cas9. *Nat Biotechnol* 2016; 34: 184-191.
434 12. Watanabe H, Ma Q, Peng S, Adelmant G, Swain D, Song W, Fox C, Francis JM, Pedamallu CS, DeLuca
435 DS, Brooks AN, Wang S, Que J, Rustgi AK, Wong KK, Ligon KL, Liu XS, Marto JA, Meyerson M, Bass

436 AJ. SOX2 and p63 colocalize at genetic loci in squamous cell carcinomas. *J Clin Invest* 2014; 124:
437 1636-1645.
438 13. Meuwissen R, Linn SC, Linnoila RI, Zevenhoven J, Mooi WJ, Berns A. Induction of small cell lung cancer
439 by somatic inactivation of both Trp53 and Rb1 in a conditional mouse model. *Cancer Cell* 2003; 4:
440 181-189.
441 14. Kusakabe T, Kawaguchi A, Hoshi N, Kawaguchi R, Hoshi S, Kimura S. Thyroid-specific enhancer-binding
442 protein/NKX2.1 is required for the maintenance of ordered architecture and function of the
443 differentiated thyroid. *Mol Endocrinol* 2006; 20: 1796-1809.
444 15. DuPage M, Dooley AL, Jacks T. Conditional mouse lung cancer models using adenoviral or lentiviral
445 delivery of Cre recombinase. *Nature protocols* 2009; 4: 1064-1072.
446 16. Zheng H, Xie W. The role of 3D genome organization in development and cell differentiation. *Nat Rev*
447 *Mol Cell Biol* 2019; 20: 535-550.
448 17. Kennedy AJ, Rahn EJ, Paulukaitis BS, Savell KE, Kordasiewicz HB, Wang J, Lewis JW, Posey J, Strange SK,
449 Guzman-Karlsson MC, Phillips SE, Decker K, Motley ST, Swayze EE, Ecker DJ, Michael TP, Day JJ,
450 Sweatt JD. Tcf4 Regulates Synaptic Plasticity, DNA Methylation, and Memory Function. *Cell Rep*
451 2016; 16: 2666-2685.
452 18. Campbell JD, Alexandrov A, Kim J, Wala J, Berger AH, Pedamallu CS, Shukla SA, Guo G, Brooks AN,
453 Murray BA, Imielinski M, Hu X, Ling S, Akbani R, Rosenberg M, Cibulskis C, Ramachandran A,
454 Collisson EA, Kwiatkowski DJ, Lawrence MS, Weinstein JN, Verhaak RG, Wu CJ, Hammerman PS,
455 Cherniack AD, Getz G, Cancer Genome Atlas Research N, Artyomov MN, Schreiber R, Govindan R,
456 Meyerson M. Distinct patterns of somatic genome alterations in lung adenocarcinomas and
457 squamous cell carcinomas. *Nat Genet* 2016; 48: 607-616.
458 19. Watanabe H, Francis JM, Woo MS, Etemad B, Lin W, Fries DF, Peng S, Snyder EL, Tata PR, Izzo F, Schinzel
459 AC, Cho J, Hammerman PS, Verhaak RG, Hahn WC, Rajagopal J, Jacks T, Meyerson M. Integrated
460 cistromic and expression analysis of amplified NKX2-1 in lung adenocarcinoma identifies LMO3 as
461 a functional transcriptional target. *Genes Dev* 2013; 27: 197-210.
462 20. Snyder EL, Watanabe H, Magendantz M, Hoersch S, Chen TA, Wang DG, Crowley D, Whittaker CA,
463 Meyerson M, Kimura S, Jacks T. Nkx2-1 represses a latent gastric differentiation program in lung
464 adenocarcinoma. *Mol Cell* 2013; 50: 185-199.
465 21. Peifer M, Fernandez-Cuesta L, Sos ML, George J, Seidel D, Kasper LH, Plenker D, Leenders F, Sun R,
466 Zander T, Menon R, Koker M, Dahmen I, Muller C, Di Cerbo V, Schildhaus HU, Altmuller J,
467 Baessmann I, Becker C, de Wilde B, Vandesompele J, Bohm D, Ansen S, Gabler F, Wilkening I,
468 Heynck S, Heuckmann JM, Lu X, Carter SL, Cibulskis K, Banerji S, Getz G, Park KS, Rauh D, Grutter
469 C, Fischer M, Pasqualucci L, Wright G, Wainer Z, Russell P, Petersen I, Chen Y, Stoelben E, Ludwig
470 C, Schnabel P, Hoffmann H, Muley T, Brockmann M, Engel-Riedel W, Muscarella LA, Fazio VM,
471 Groen H, Timens W, Sietsma H, Thunnissen E, Smit E, Heideman DA, Snijders PJ, Cappuzzo F,
472 Ligorio C, Damiani S, Field J, Solberg S, Brustugun OT, Lund-Iversen M, Sanger J, Clement JH,
473 Soltermann A, Moch H, Weder W, Solomon B, Soria JC, Validire P, Besse B, Brambilla E, Brambilla
474 C, Lantuejoul S, Lorimier P, Schneider PM, Hallek M, Pao W, Meyerson M, Sage J, Shendure J,
475 Schneider R, Buttner R, Wolf J, Nurnberg P, Perner S, Heukamp LC, Brindle PK, Haas S, Thomas RK.
476 Integrative genome analyses identify key somatic driver mutations of small-cell lung cancer. *Nat*
477 *Genet* 2012; 44: 1104-1110.
478 22. Horie M, Miyashita N, Mattsson JSM, Mikami Y, Sandelin M, Brunnstrom H, Micke P, Nagase T, Saito
479 A. An integrative transcriptome analysis reveals a functional role for thyroid transcription factor-
480 1 in small cell lung cancer. *J Pathol* 2018; 246: 154-165.
481 23. Misch D, Blum T, Boch C, Weiss T, Crolow C, Griff S, Mairinger T, Bauer TT, Kollmeier J. Value of thyroid
482 transcription factor (TTF)-1 for diagnosis and prognosis of patients with locally advanced or
483 metastatic small cell lung cancer. *Diagn Pathol* 2015; 10: 21.

484 24. Miyauchi E, Motoi N, Ono H, Ninomiya H, Ohyanagi F, Nishio M, Okumura S, Ichinose M, Ishikawa Y.
485 Distinct Characteristics of Small Cell Lung Cancer Correlate With Central or Peripheral Origin:
486 Subtyping Based on Location and Expression of Transcription Factor TTF-1. *Medicine (Baltimore)*
487 2015; 94: e2324.
488 25. Wu M, Wang B, Gil J, Sabo E, Miller L, Gan L, Burstein DE. p63 and TTF-1 immunostaining. A useful
489 marker panel for distinguishing small cell carcinoma of lung from poorly differentiated squamous
490 cell carcinoma of lung. *Am J Clin Pathol* 2003; 119: 696-702.
491 26. Ordonez NG. Value of thyroid transcription factor-1 immunostaining in distinguishing small cell lung
492 carcinomas from other small cell carcinomas. *Am J Surg Pathol* 2000; 24: 1217-1223.
493 27. Jiang L, Huang J, Higgs BW, Hu Z, Xiao Z, Yao X, Conley S, Zhong H, Liu Z, Brohawn P, Shen D, Wu S, Ge
494 X, Jiang Y, Zhao Y, Lou Y, Morehouse C, Zhu W, Sebastian Y, Czapiga M, Oganesyan V, Fu H, Niu Y,
495 Zhang W, Streicher K, Tice D, Zhao H, Zhu M, Xu L, Herbst R, Su X, Gu Y, Li S, Huang L, Gu J, Han B,
496 Jallal B, Shen H, Yao Y. Genomic Landscape Survey Identifies SRSF1 as a Key Oncodriver in Small
497 Cell Lung Cancer. *PLoS Genet* 2016; 12: e1005895.
498 28. Weir BA, Woo MS, Getz G, Perner S, Ding L, Beroukhim R, Lin WM, Province MA, Kraja A, Johnson LA,
499 Shah K, Sato M, Thomas RK, Barletta JA, Borecki IB, Broderick S, Chang AC, Chiang DY, Chirieac LR,
500 Cho J, Fujii Y, Gazdar AF, Giordano T, Greulich H, Hanna M, Johnson BE, Kris MG, Lash A, Lin L,
501 Lindeman N, Mardis ER, McPherson JD, Minna JD, Morgan MB, Nadel M, Orringer MB, Osborne
502 JR, Ozenberger B, Ramos AH, Robinson J, Roth JA, Rusch V, Sasaki H, Shepherd F, Sougnez C, Spitz
503 MR, Tsao MS, Twomey D, Verhaak RG, Weinstock GM, Wheeler DA, Winckler W, Yoshizawa A, Yu
504 S, Zakowski MF, Zhang Q, Beer DG, Wistuba, II, Watson MA, Garraway LA, Ladanyi M, Travis WD,
505 Pao W, Rubin MA, Gabriel SB, Gibbs RA, Varmus HE, Wilson RK, Lander ES, Meyerson M.
506 Characterizing the cancer genome in lung adenocarcinoma. *Nature* 2007; 450: 893-898.
507 29. Hokari S, Tamura Y, Kaneda A, Katsura A, Morikawa M, Murai F, Ehata S, Tsutsumi S, Ishikawa Y,
508 Aburatani H, Kikuchi T, Miyazono K, Koinuma D. Comparative analysis of TTF-1-binding DNA
509 regions in small cell lung cancer and non-small cell lung cancer. *Mol Oncol* 2019.
510 30. Heinz S, Romanoski CE, Benner C, Glass CK. The selection and function of cell type-specific enhancers.
511 *Nat Rev Mol Cell Biol* 2015; 16: 144-154.
512 31. Magno L, Barry C, Schmidt-Hieber C, Theodotou P, Hausser M, Kessaris N. NKX2-1 Is Required in the
513 Embryonic Septum for Cholinergic System Development, Learning, and Memory. *Cell Rep* 2017;
514 20: 1572-1584.
515 32. Liu Y, Bhowmick T, Liu Y, Gao X, Mertens HDT, Svergun DI, Xiao J, Zhang Y, Wang JH, Meijers R.
516 Structural Basis for Draxin-Modulated Axon Guidance and Fasciculation by Netrin-1 through DCC.
517 *Neuron* 2018; 97: 1261-1267 e1264.
518 33. Saint-Andre V, Federation AJ, Lin CY, Abraham BJ, Reddy J, Lee TI, Bradner JE, Young RA. Models of
519 human core transcriptional regulatory circuitries. *Genome Res* 2016; 26: 385-396.
520 34. Reissner C, Runkel F, Missler M. Neurexins. *Genome Biol* 2013; 14: 213.
521 35. Sudhof TC. Neuroligins and neurexins link synaptic function to cognitive disease. *Nature* 2008; 455:
522 903-911.
523 36. Toma C, Torrico B, Hervas A, Valdes-Mas R, Tristan-Noguero A, Padillo V, Maristany M, Salgado M,
524 Arenas C, Puente XS, Bayes M, Cormand B. Exome sequencing in multiplex autism families
525 suggests a major role for heterozygous truncating mutations. *Mol Psychiatry* 2014; 19: 784-790.
526 37. Wu Z, Zhou J, Zhang X, Zhang Z, Xie Y, Liu JB, Ho ZV, Panda A, Qiu X, Cejas P, Canadas I, Akarca FG,
527 McFarland JM, Nagaraja AK, Goss LB, Kesten N, Si L, Lim K, Liu Y, Zhang Y, Baek JY, Liu Y, Patil DT,
528 Katz JP, Hai J, Bao C, Stachler M, Qi J, Ishizuka JJ, Nakagawa H, Rustgi AK, Wong KK, Meyerson M,
529 Barbie DA, Brown M, Long H, Bass AJ. Reprogramming of the esophageal squamous carcinoma
530 epigenome by SOX2 promotes ADAR1 dependence. *Nat Genet* 2021; 53: 881-894.

531 38. Borromeo MD, Savage TK, Kollipara RK, He M, Augustyn A, Osborne JK, Girard L, Minna JD, Gazdar AF,
532 Cobb MH, Johnson JE. ASCL1 and NEUROD1 Reveal Heterogeneity in Pulmonary Neuroendocrine
533 Tumors and Regulate Distinct Genetic Programs. *Cell Rep* 2016; 16: 1259-1272.
534 39. Olsen RR, Ireland AS, Kastner DW, Groves SM, Spainhower KB, Pozo K, Kelenis DP, Whitney CP, Guthrie
535 MR, Wait SJ, Soltero D, Witt BL, Quaranta V, Johnson JE, Oliver TG. ASCL1 represses a SOX9(+)
536 neural crest stem-like state in small cell lung cancer. *Genes Dev* 2021; 35: 847-869.
537 40. La Rosa S, Chiaravalli AM, Placidi C, Papanikolaou N, Cerati M, Capella C. TTF1 expression in normal
538 lung neuroendocrine cells and related tumors: immunohistochemical study comparing two
539 different monoclonal antibodies. *Virchows Arch* 2010; 457: 497-507.
540 41. Yamaguchi T, Hosono Y, Yanagisawa K, Takahashi T. NKX2-1/TTF-1: an enigmatic oncogene that
541 functions as a double-edged sword for cancer cell survival and progression. *Cancer Cell* 2013; 23:
542 718-723.
543 42. Puelles L, Kuwana E, Puelles E, Bulfone A, Shimamura K, Keleher J, Smiga S, Rubenstein JL. Pallial and
544 subpallial derivatives in the embryonic chick and mouse telencephalon, traced by the expression
545 of the genes Dlx-2, Emx-1, Nkx-2.1, Pax-6, and Tbr-1. *J Comp Neurol* 2000; 424: 409-438.
546 43. Flames N, Pla R, Gelman DM, Rubenstein JL, Puelles L, Marin O. Delineation of multiple subpallial
547 progenitor domains by the combinatorial expression of transcriptional codes. *J Neurosci* 2007; 27:
548 9682-9695.
549 44. Sussel L, Marin O, Kimura S, Rubenstein JL. Loss of Nkx2.1 homeobox gene function results in a ventral
550 to dorsal molecular respecification within the basal telencephalon: evidence for a transformation
551 of the pallidum into the striatum. *Development* 1999; 126: 3359-3370.
552 45. Minocha S, Valloton D, Ypsilanti AR, Fiumelli H, Allen EA, Yanagawa Y, Marin O, Chedotal A, Hornung
553 JP, Lebrand C. Nkx2.1-derived astrocytes and neurons together with Slit2 are indispensable for
554 anterior commissure formation. *Nat Commun* 2015; 6: 6887.
555 46. Cardnell RJ, Li L, Sen T, Bara R, Tong P, Fujimoto J, Ireland AS, Guthrie MR, Bheddah S, Banerjee U, Kalu
556 NN, Fan YH, Dylla SJ, Johnson FM, Wistuba, II, Oliver TG, Heymach JV, Glisson BS, Wang J, Byers
557 LA. Protein expression of TTF1 and cMYC define distinct molecular subgroups of small cell lung
558 cancer with unique vulnerabilities to aurora kinase inhibition, DLL3 targeting, and other targeted
559 therapies. *Oncotarget* 2017; 8: 73419-73432.
560 47. Camolotto SA, Pattabiraman S, Mosbruger TL, Jones A, Belova VK, Orstad G, Streiff M, Salmond L,
561 Stubben C, Kaestner KH, Snyder EL. FoxA1 and FoxA2 drive gastric differentiation and suppress
562 squamous identity in NKX2-1-negative lung cancer. *Elife* 2018; 7.
563 48. Zewdu R, Mehrabad EM, Ingram K, Fang P, Gillis KL, Camolotto SA, Orstad G, Jones A, Mendoza MC,
564 Spike BT, Snyder EL. An NKX2-1/ERK/WNT feedback loop modulates gastric identity and response
565 to targeted therapy in lung adenocarcinoma. *Elife* 2021; 10.

566

567 **Figure legends**

568 **Figure 1. Epigenomic profiling subdivided SCLC-A by differential super-enhancers**

569 (**A**). Unsupervised hierarchical clustering of 25 SCLC cell lines using SE signals near
570 transcriptional regulator genes. The color scale indicates the intensity of SE signals normalized to
571 linear scores using the sum of squares of the values. Each row represents a SE locus (747 loci).
572 The color shades on the dendrogram indicate four novel SE clusters, the top red columns display
573 the presence of SE near the *NKX2-1* locus, and the bottom column colors denote the consensus
574 expression clusters. (**B**). Volcano plot showing 140 differentially enriched SEs (110 enriched in
575 SCLC-Aα and 30 enriched in SCLC-Aσ) at thresholds of absolute fold change ≥ 5 and FDR ≤ 0.25
576 depicted as dotted lines. (**C**). Genome view tracks of H3K27ac signal at the *NKX2-1* locus in four
577 clusters of SCLC cell lines. Normalized scales are shown in Figure E1B. (**D**). SE plots with all
578 enhancers rank-ordered by H3K27ac signals in DMS 79, NCI-H187, NCI-H209 and NCI-H345.
579 Dotted lines depict tangential cutoffs to define SEs. (**E**). Genome view tracks of H3K27ac signals
580 at the *ASCL1*, *NEUROD1*, *POU2F3*, *YAP1* and *NKX2-1* loci in 2 human SCLC specimens of
581 SCLC-A subtype. (**F**). Protein expression of NKX2-1, ASCL1 and vinculin as a loading control in
582 SCLC cell lines from different clusters. *NKX2-1*-amplified adenocarcinoma cell lines NCI-H3122
583 and NCI-H2087 are shown as reference. (**G**). Box and jitter plots showing the distribution of
584 *NKX2-1* mRNA expression in SCLC-A, SCLC-N, SCLC-P, and SCLC-Y subtypes of 135 primary
585 SCLC tumors.

586 **Figure 2. *NKX2-1* survival dependency is unique to SCLC-Aα**

587 (**A**). *(Top)* Immunoblots showing protein expression of NKX2-1 and vinculin as a loading control
588 in SCLC-Aα cell lines with three *NKX2-1* sgRNAs, or two non-target (NT) sgRNAs. *(Bottom)*

589 Cell growth curve for SCLC-Aα cell lines infected with *NKX2-1* sgRNAs or NT sgRNAs. Data
590 are shown as mean ± SD (n=3); *P < 0.0001 by two-sided two-way ANOVA. (**B**). *(Top)*
591 Immunoblots showing protein expression of NKX2-1 and vinculin as a loading control in SCLC-
592 Aσ (NCI-H2171, NCI-H69) and SCLC-N (NCI-H1963) cell lines with *NKX2-1* sgRNAs, or non-
593 target (NT) sgRNAs. *(Bottom)* Cell growth curve for cell lines infected with *NKX2-1* sgRNA or
594 NT sgRNAs. Data are shown as mean ± SD (n=3); *P < 0.0001 by two-sided two-way ANOVA.
595 (**C**). Bar plots showing percentage of apoptotic NCI-H187 cells infected with NT sgRNA and
596 *NKX2-1* sgRNA, measured by annexin V staining. Means ± SD of three biological replicates. *P
597 < 0.0001, t test. Representative data for NT sg1 and NKX2-1 sg1 can be found in Figure E2A. (**D**).
598 (*Left*) Tumor growth curve for xenograft tumors of NCI-H187 cells infected with *NKX2-1* sg1 or
599 NT sg1 *in vivo*. Mean ± SD of four biological replicates. *P < 0.0001, t test. Xenograft tumors were
600 resected at 3 weeks after inoculation. (*Right*) Images of resected xenograft tumors of NCI-H209
601 cells infected with NT sg1 or *NKX2-1* sg1 *in vivo* at day 23.

602 **Figure 3. Genomic occupancy of *NKX2-1* in SCLC-Aα cells distinct from that in LADC cells**

603 (**A**). Correlation matrix depicting pairwise comparisons of identified NKX2-1 binding peaks in the
604 5 SCLC-Aα cell lines and in 3 LADC cell lines. Color scale represents degree of Pearson's
605 correlation coefficient. (**B**). Heatmap showing signals from NKX2-1 ChIP-seq data in the 5 SCLC-
606 Aα cell lines and 3 LUAC cell lines. ChIP signal intensity is shown by red shading. Y-axis contains
607 all peaks that are bound by NKX2-1 in any of SCLC-Aα and LUAC (n=37,198). Peaks are divided
608 into 4 regions by *k-means* (k=4) clustering. (**C**). NKX2-1 ChIP-seq signals in SCLC-Aα and
609 LADC cell lines at representative loci (*RUNX1*; cluster 1, *LMO3*; cluster 3 and *DCC*; cluster 2).
610 Red: SCLC-Aα cell lines. Black: LADC cell lines. (**D**). Heatmap showing 2,671 differentially
611 NKX2-1 bound regions (fold change $\geq 2^5$ and FDR $\leq 1\text{x}10^{-5}$), 2,010 enriched in LADC and 661

612 enriched in SCLC-Aα, between 5 SCLC-Aα cell lines and 3 LUAC cell lines. (**E**). Enriched
613 ontology by GREAT analyses for regions differentially bound by NKX2-1 in 5 SCLC-Aα
614 compared to LADCs.

615 **Figure 4. NKX2-1 interactome in chromatin of SCLC-Aα cells includes SOX1**

616 (**A**). Experimental strategy to identify binding partners of NKX2-1 in SCLC-Aα. Chromatin
617 prepared from the nuclear fraction of SCLC-Aα cell lines NCI-H187 and NCI-H1436 stably
618 expressing FLAG-NKX2-1 was solubilized using micrococcal nuclease digestion. Co-
619 immunoprecipitated proteins with anti-FLAG antibody from solubilized chromatin were identified
620 by LC-MS/MS (see Data file S2 for the complete list). (**B**). Venn diagram showing the number of
621 transcription factors identified in each of the 2 SCLC-Aα cell lines and the 27 overlaps found in
622 both cell lines. The proteins indicated in yellow color were also found in CRC analysis in Figure
623 4C. (**C**). Core transcriptional regulatory circuitries (CRCs) commonly identified in 8 SCLC-Aα
624 cell lines. The genes in yellow color were also found in LC-MS/MS analysis in Figure 4B. (**D**).
625 Genome view tracks of H3K27ac signal at the *SOX1* locus in four clusters of SCLC cell lines. (**E**).
626 Immunoblots with anti-SOX1 antibody on endogenous co-immunoprecipitates by anti-NKX2-1
627 antibody in SCLC-Aα (DMS 79 and NCI-H187) cells. (**F**). *In situ* proximity ligation assay signals
628 (red fluorescence) targeting endogenous SOX1 and NKX2-1 in NCI-H841, NCI-H187, NCI-H209
629 and DMS 79 cells. Nuclei are counterstained with DAPI (blue). See Figure E4G for additional
630 control.

631 **Figure 5. NKX2-1 and SOX1 co-occupy the SCLC-Aα genome to collaborate in gene**
632 **regulation**

633 (**A**). Heatmap showing k-means clustering (*k*=4) of signals at the common 4,051 loci from NKX2-
634 1 (red) and SOX1 (blue) ChIP-seq data in the 4 SCLC-Aα cell lines. ChIP signal intensity is shown
635 by shading for all NKX2-1 and SOX1 occupied loci. (**B**). Venn diagram showing the overlap of
636 NKX2-1 common binding sites and SOX1 common binding sites present in at least 3 SCLC-Aα
637 cell lines. (**C**). Genome view tracks of NKX2-1 (red) and SOX1 (blue) ChIP-seq signals in four
638 SCLC-Aα (DMS 79, NCI-H187, NCI-H209 and NCI-H345) cell lines and 3 LADC cell lines at
639 the representative NKX2-1-SOX1 co-occupied loci (*NRXN3* and *YWHAZ*; SCLC-Aα unique,
640 *NKX2-1*; SCLC-Aα/LADC common). (**D**). Enriched ontology by GREAT analyses for regions in
641 604 overlapping high-confidence NKX2-1-SOX1 binding sites.

642 **Figure 6. Collaboration of NKX2-1 and SOX1 is required to control the neuronal state in**
643 **SCLC-Aα**

644 (**A**). Venn diagram showing the overlap of downregulated genes after depletion of NKX2-1 (fold
645 change > 1.4 and adjusted P < 0.05) and SOX1 (fold change > 2 and adjusted P < 0.05) in NCI-
646 H187 cells. (**B**). Gene Set Enrichment Analysis (GSEA) of genes associated with 2,652 NKX2-1-
647 SOX1 co-occupied loci for expression data upon repression of NKX2-1 (*left*) or SOX1 (*right*) in
648 NCI-H187 cells, with their leading-edge genes shaded. Enrichment was significant for both (NES=
649 -2.29, P < 0.001 for NKX2-1 and NES= -2.54, P < 0.001 for SOX1). (**C**). Enriched gene ontologies
650 (MSigDB, biological process) for 289 common genes in leading-edge genes for both NKX2-1 and
651 SOX1 deletions. (**D**). Correlation matrix depicting pairwise comparisons of identified NKX2-1
652 binding regions in three *SOX1* sgRNAs and three control cells (two non-target (NT) sgRNAs, one
653 parental cell) of NCI-H187 cell line. Color scale represents degree of Pearson's correlation
654 coefficient. (**E**). Heatmap showing k-means clustering (*k*=4) of 2,067 NKX2-1 ChIP-seq loci in
655 NCI-H187 sgSOX1 compared to control cells with reduced signal intensity. ChIP-seq signal

656 intensity is shown by color shading. (**F**). Average H3K27ac ChIP-seq signals on NKX2-1 reduced
657 binding sites and NKX2-1 non-reduced binding sites defined in Figure E6D for NCI-H187 parental,
658 NT sg1, SOX1 sg2 and SOX1 sg3 cells.

659 **Figure 7. *Nkx2-1* is essential for development of SCLC-Aα tumors in an autochthonous**
660 **mouse model**

661 (**A**). Genetically engineered mouse models of SCLCs. *Rb1*$^{flox/flox}$; *Trp53*$^{flox/flox}$ (RP) mice or
662 *Rb1*$^{flox/flox}$; *Trp53*$^{flox/flox}$, *Nkx2-1* $^{flox/flox}$ (RPN) mice were transduced with Adeno-CMV-*Cre* to
663 initiate SCLC. (**B**). Genome view tracks at the Nkx2-1, Sox1, and Ascl1 loci for H3K27ac ChIP-
664 seq signals in 10 SCLC tumors from RP mice and 10 SCLC tumors from RPN mice. * indicates 3
665 tumors that have high-level signal at both *Nkx2-1* and *Sox1* loci. The arrowheads on *Nkx2-1* locus
666 indicate the loxP sites in RPN mice**.** (**C**). Representative immune-staining images for Nkx2-1,
667 Sox1, and Ascl1 on SCLC tumors from RP and RPN mice. Scale bars, 25μm. (**D**). Representative
668 hematoxylin and eosin (H&E) images of SCLC tumors from RP and RPN mice. Scale bars, 2.5mm
669 and 50μm, respectively. (**E**). Enriched gene ontologies (MSigDB, biological process) for the
670 differentially downregulated genes in RPN tumors compared to RP tumors. (**F**). Average copy
671 number profiles in RP and RPN models. Arrows indicate the *Nfib* and *Mycl* loci that are
672 specifically amplified in RP tumors (individual copy number profiles at those loci are available in
673 Figure E8C).

Figure 1

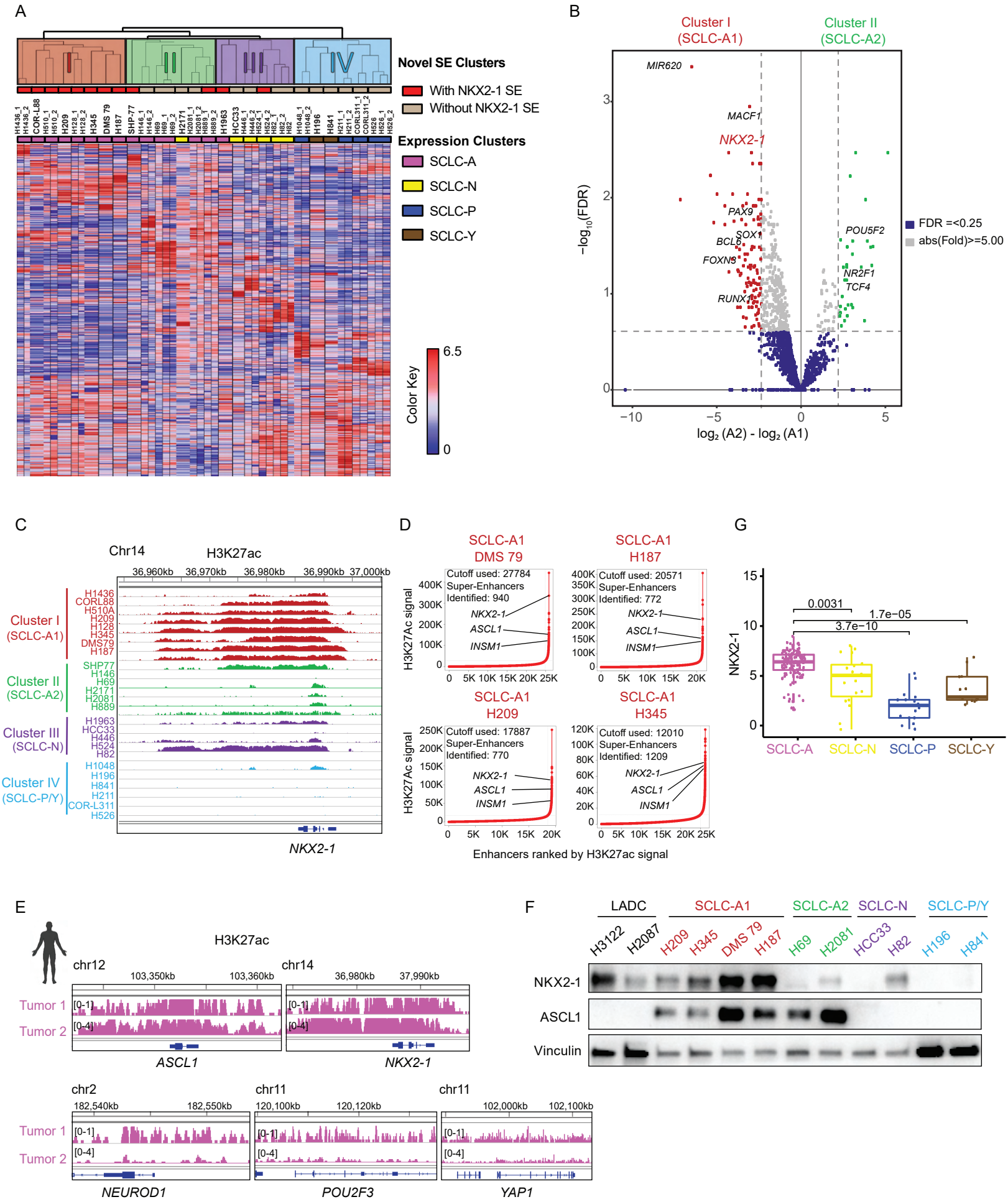
A
Novel SE Clusters
With NKX2-1 SE
Without NKX2-1 SE
Expression Clusters
SCLC-A
SCLC-N
SCLC-P
SCLC-Y
Color Key
6.5
0
B
Cluster I (SCLC-A1)
Cluster II (SCLC-A2)
MIR620
MACF1
NKX2-1
PAX9
SOX1
BCL6
FOXN3
RUNX1
POU5F2
NR2F1
TCF4
FDR =<0.25
abs(Fold)>=5.00
−log10(FDR)
log2 (A2) - log2 (A1)
C
Chr14
H3K27ac
36,960kb
36,970kb
36,980kb
36,990kb
37,000kb
Cluster I (SCLC-A1)
Cluster II (SCLC-A2)
Cluster III (SCLC-N)
Cluster IV (SCLC-P/Y)
NKX2-1
D
SCLC-A1 DMS 79
Cutoff used: 27784
Super-Enhancers Identified: 940
SCLC-A1 H187
Cutoff used: 20571
Super-Enhancers Identified: 772
SCLC-A1 H209
Cutoff used: 17887
Super-Enhancers Identified: 770
SCLC-A1 H345
Cutoff used: 12010
Super-Enhancers Identified: 1209
NKX2-1
ASCL1
INSM1
H3K27Ac signal
Enhancers ranked by H3K27ac signal
G
NKX2-1
0.0031
1.7e−05
3.7e−10
SCLC-A
SCLC-N
SCLC-P
SCLC-Y
E
H3K27ac
chr12
103,350kb
103,360kb
chr14
36,980kb
37,990kb
Tumor 1
Tumor 2
ASCL1
NKX2-1
chr2
182,540kb
182,550kb
chr11
120,100kb
120,120kb
chr11
102,000kb
102,100kb
NEUROD1
POU2F3
YAP1
F
LADC
SCLC-A1
SCLC-A2
SCLC-N
SCLC-P/Y
H3122
H2087
H209
H345
DMS 79
H187
H69
H2081
HCC33
H82
H196
H841
NKX2-1
ASCL1
Vinculin

Figure 2

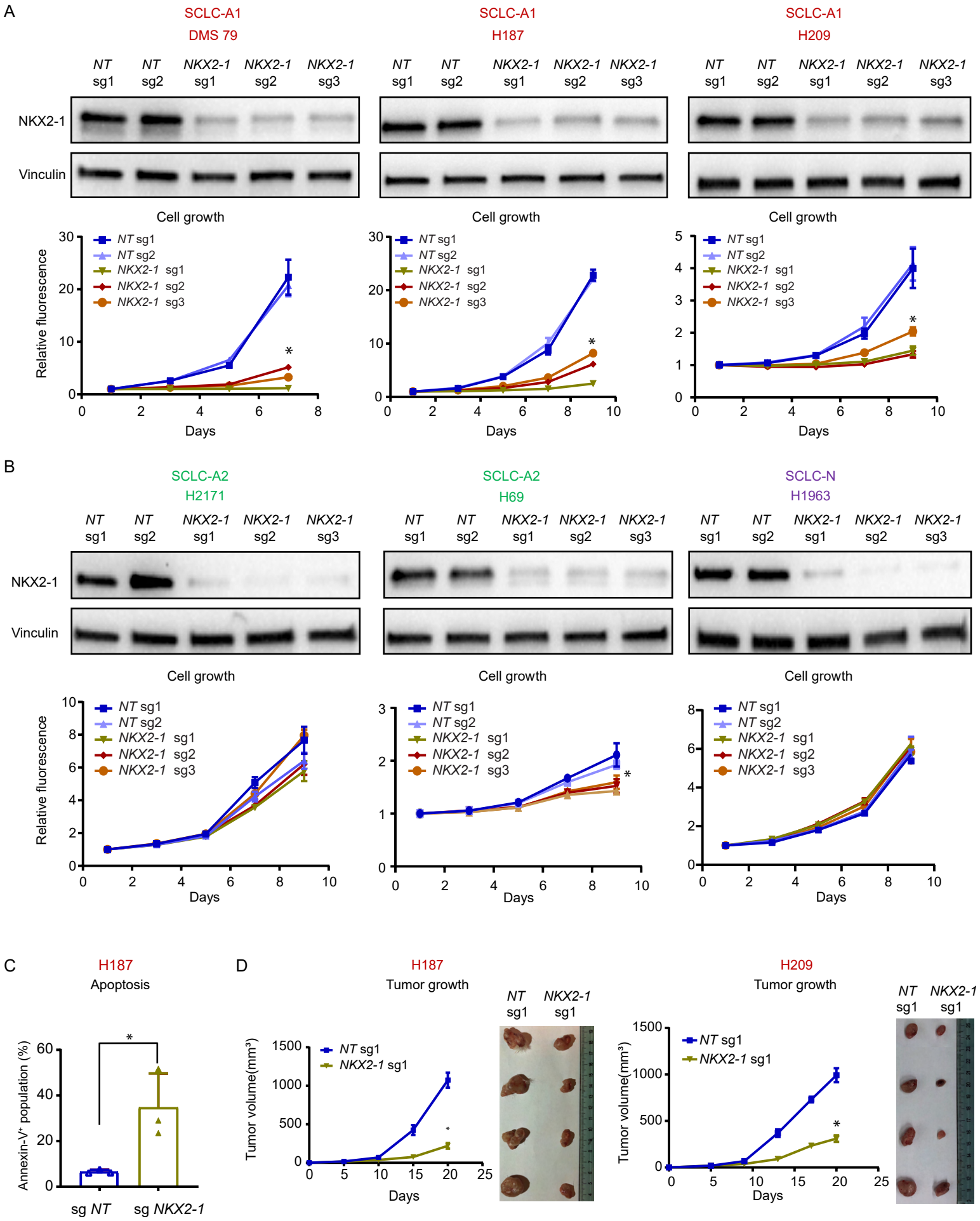
A
SCLC-A1
DMS 79
SCLC-A1
H187
SCLC-A1
H209
NT sg1
NT sg2
NKX2-1 sg1
NKX2-1 sg2
NKX2-1 sg3
NKX2-1
Vinculin
Cell growth
Relative fluorescence
Days
B
SCLC-A2
H2171
SCLC-A2
H69
SCLC-N
H1963
C
H187
Apoptosis
Annexin-V+ population (%)
sg NT
sg NKX2-1
D
H187
Tumor growth
Tumor volume(mm³)
H209
Tumor growth

Figure 3

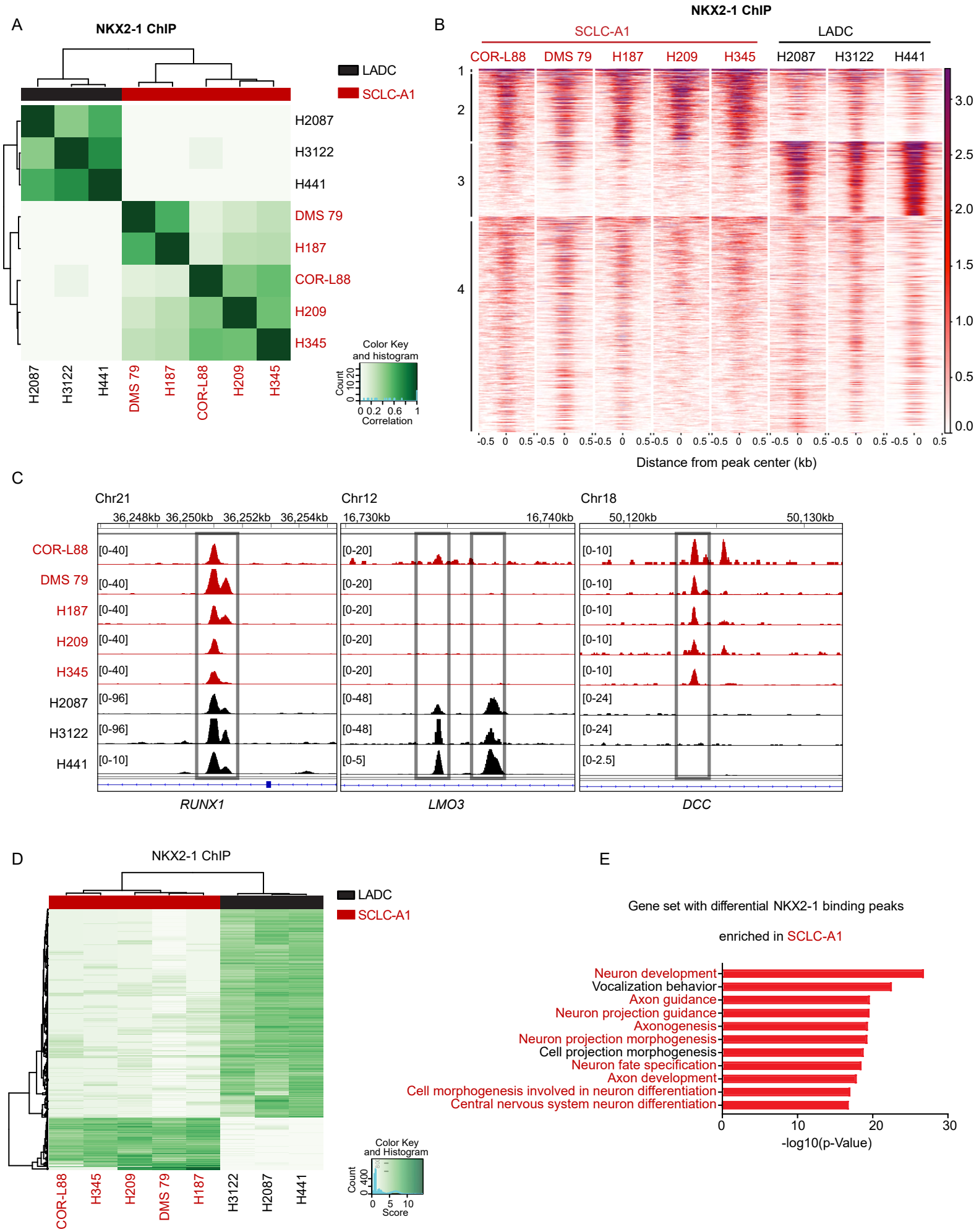
A
NKX2-1 ChIP
LADC
SCLC-A1
H2087
H3122
H441
DMS 79
H187
COR-L88
H209
H345
Color Key and histogram
Count
Correlation
B
NKX2-1 ChIP
SCLC-A1
LADC
COR-L88
DMS 79
H187
H209
H345
H2087
H3122
H441
Distance from peak center (kb)
C
Chr21
Chr12
Chr18
36,248kb 36,250kb 36,252kb 36,254kb
16,730kb 16,740kb
50,120kb 50,130kb
COR-L88
DMS 79
H187
H209
H345
H2087
H3122
H441
RUNX1
LMO3
DCC
D
NKX2-1 ChIP
LADC
SCLC-A1
COR-L88
H345
H209
DMS 79
H187
H3122
H2087
H441
Color Key and Histogram
Count
Score
E
Gene set with differential NKX2-1 binding peaks
enriched in SCLC-A1
Neuron development
Vocalization behavior
Axon guidance
Neuron projection guidance
Axonogenesis
Neuron projection morphogenesis
Cell projection morphogenesis
Neuron fate specification
Axon development
Cell morphogenesis involved in neuron differentiation
Central nervous system neuron differentiation
-log10(p-Value)

Figure 4

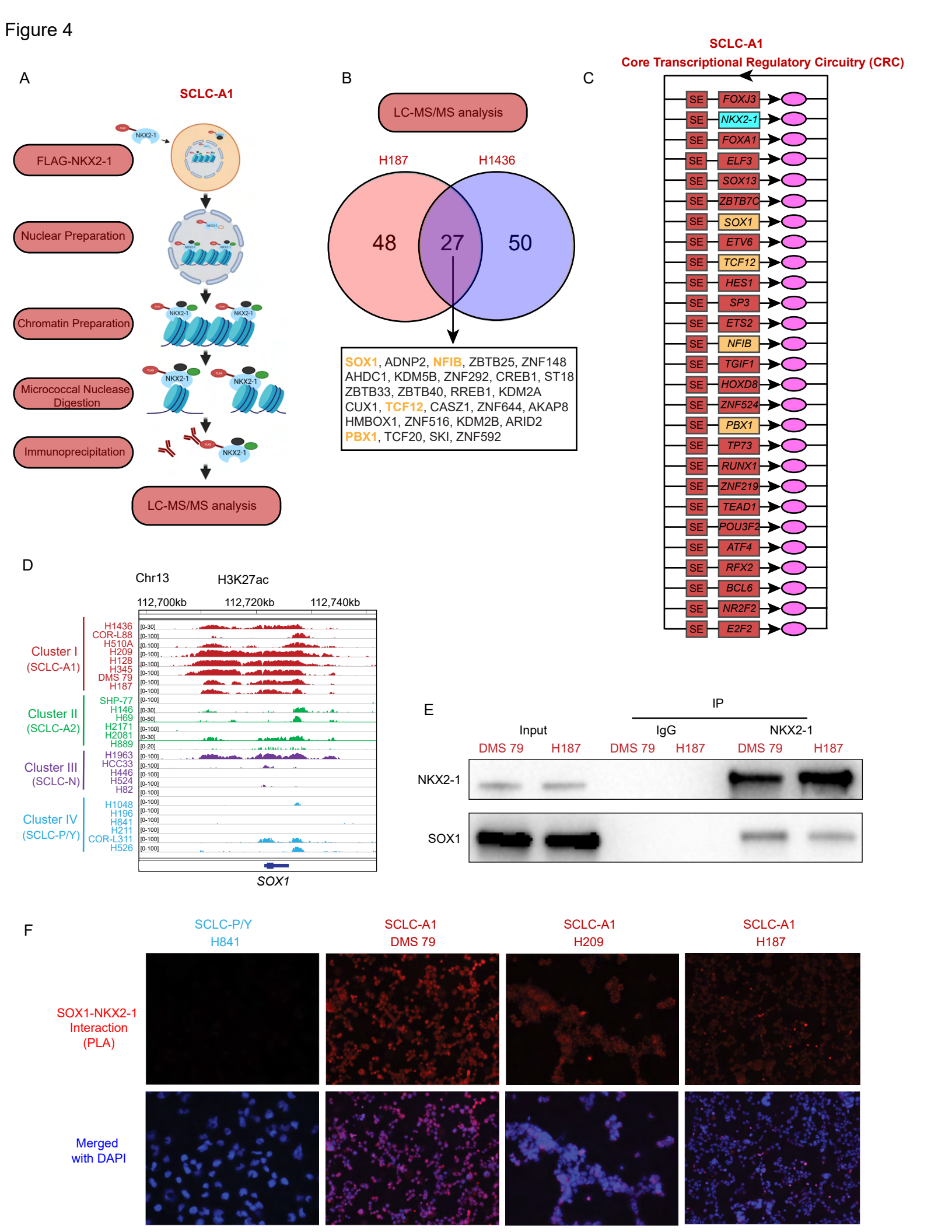
A
SCLC-A1
FLAG-NKX2-1
Nuclear Preparation
Chromatin Preparation
Micrococcal Nuclease Digestion
Immunoprecipitation
LC-MS/MS analysis
B
LC-MS/MS analysis
H187
H1436
48
27
50
SOX1, ADNP2, NFIB, ZBTB25, ZNF148
AHDC1, KDM5B, ZNF292, CREB1, ST18
ZBTB33, ZBTB40, RREB1, KDM2A
CUX1, TCF12, CASZ1, ZNF644, AKAP8
HMBOX1, ZNF516, KDM2B, ARID2
PBX1, TCF20, SKI, ZNF592
C
SCLC-A1
Core Transcriptional Regulatory Circuitry (CRC)
SE FOXJ3
SE NKX2-1
SE FOXA1
SE ELF3
SE SOX13
SE ZBTB7C
SE SOX1
SE ETV6
SE TCF12
SE HES1
SE SP3
SE ETS2
SE NFIB
SE TGIF1
SE HOXD8
SE ZNF524
SE PBX1
SE TP73
SE RUNX1
SE ZNF219
SE TEAD1
SE POU3F2
SE ATF4
SE RFX2
SE BCL6
SE NR2F2
SE E2F2
D
Chr13
H3K27ac
112,700kb
112,720kb
112,740kb
Cluster I (SCLC-A1)
H1436
COR-L88
H510A
H209
H128
H345
DMS 79
H187
Cluster II (SCLC-A2)
SHP-77
H146
H69
H2171
H2081
H889
Cluster III (SCLC-N)
H1963
HCC33
H446
H524
H82
Cluster IV (SCLC-P/Y)
H1048
H196
H841
H211
COR-L311
H526
SOX1
E
IP
Input
IgG
NKX2-1
DMS 79
H187
DMS 79
H187
DMS 79
H187
NKX2-1
SOX1
F
SCLC-P/Y
H841
SCLC-A1
DMS 79
SCLC-A1
H209
SCLC-A1
H187
SOX1-NKX2-1 Interaction (PLA)
Merged with DAPI

Figure 5

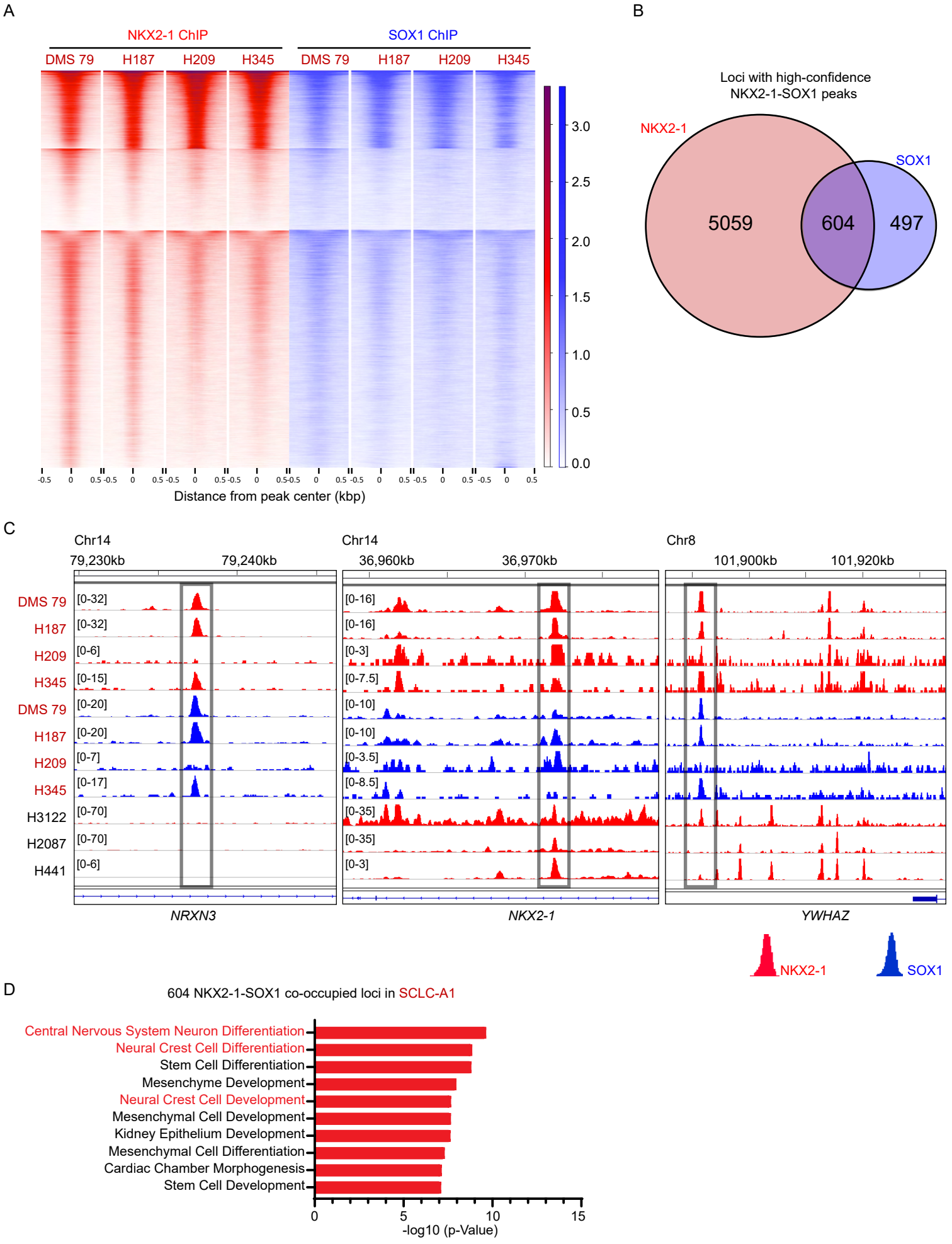
A
NKX2-1 ChIP
SOX1 ChIP
DMS 79
H187
H209
H345
DMS 79
H187
H209
H345
3.0
2.5
2.0
1.5
1.0
0.5
0.0
-0.5
0
0.5
Distance from peak center (kbp)
B
Loci with high-confidence
NKX2-1-SOX1 peaks
NKX2-1
SOX1
5059
604
497
C
Chr14
79,230kb
79,240kb
Chr14
36,960kb
36,970kb
Chr8
101,900kb
101,920kb
DMS 79
H187
H209
H345
DMS 79
H187
H209
H345
H3122
H2087
H441
[0-32]
[0-32]
[0-6]
[0-15]
[0-20]
[0-20]
[0-7]
[0-17]
[0-70]
[0-70]
[0-6]
[0-16]
[0-16]
[0-3]
[0-7.5]
[0-10]
[0-10]
[0-3.5]
[0-8.5]
[0-35]
[0-35]
[0-3]
NRXN3
NKX2-1
YWHAZ
NKX2-1
SOX1
D
604 NKX2-1-SOX1 co-occupied loci in SCLC-A1
Central Nervous System Neuron Differentiation
Neural Crest Cell Differentiation
Stem Cell Differentiation
Mesenchyme Development
Neural Crest Cell Development
Mesenchymal Cell Development
Kidney Epithelium Development
Mesenchymal Cell Differentiation
Cardiac Chamber Morphogenesis
Stem Cell Development
0
5
10
15
-log10 (p-Value)

Figure 6

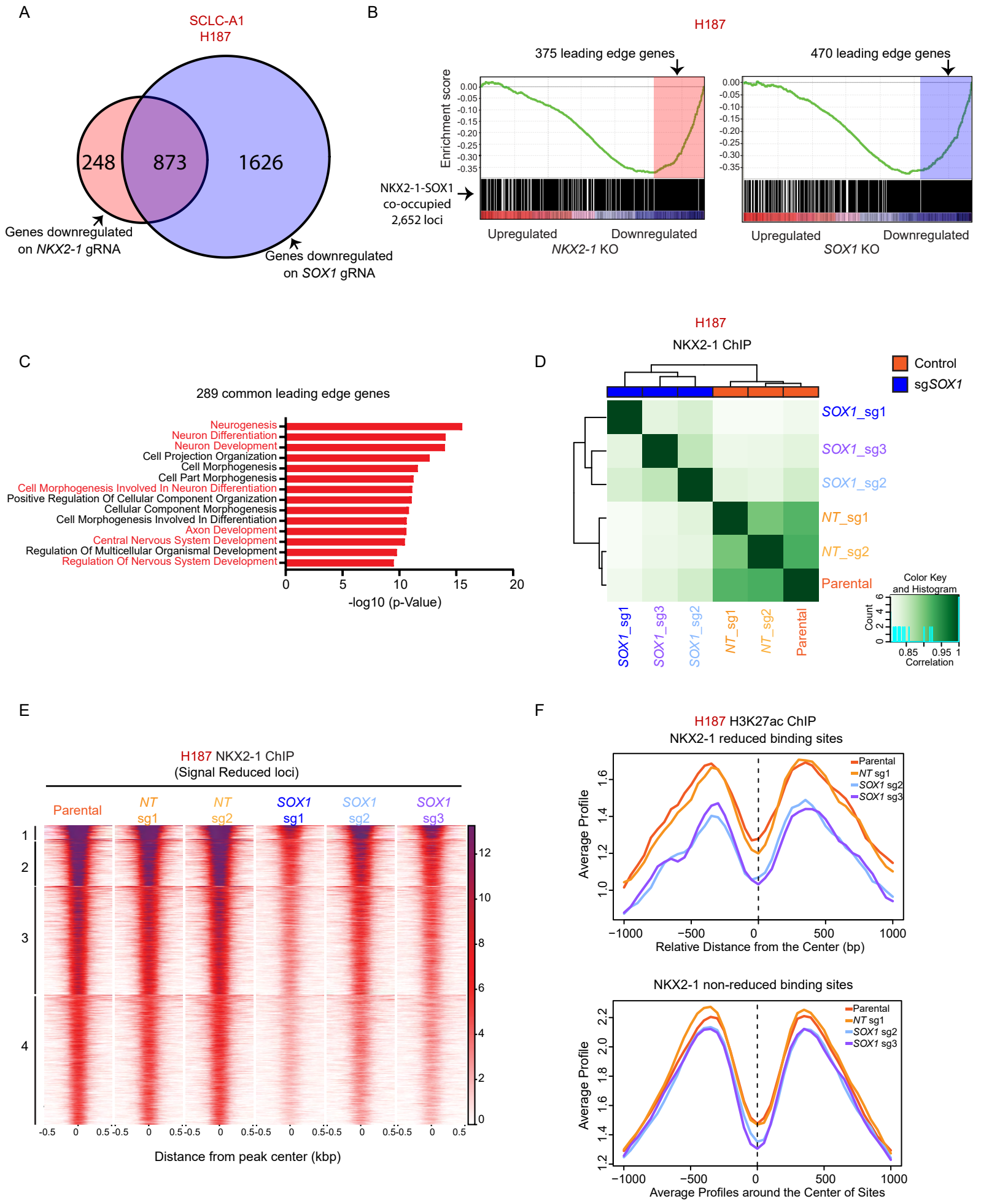
A
SCLC-A1
H187
248
873
1626
Genes downregulated on NKX2-1 gRNA
Genes downregulated on SOX1 gRNA
B
H187
375 leading edge genes
470 leading edge genes
Enrichment score
NKX2-1-SOX1 co-occupied 2,652 loci
Upregulated
Downregulated
NKX2-1 KO
SOX1 KO
C
289 common leading edge genes
Neurogenesis
Neuron Differentiation
Neuron Development
Cell Projection Organization
Cell Morphogenesis
Cell Part Morphogenesis
Cell Morphogenesis Involved In Neuron Differentiation
Positive Regulation Of Cellular Component Organization
Cellular Component Morphogenesis
Cell Morphogenesis Involved In Differentiation
Axon Development
Central Nervous System Development
Regulation Of Multicellular Organismal Development
Regulation Of Nervous System Development
-log10 (p-Value)
D
H187
NKX2-1 ChIP
Control
sgSOX1
SOX1_sg1
SOX1_sg3
SOX1_sg2
NT_sg1
NT_sg2
Parental
Color Key and Histogram
Count
Correlation
E
H187 NKX2-1 ChIP
(Signal Reduced loci)
Parental
NT sg1
NT sg2
SOX1 sg1
SOX1 sg2
SOX1 sg3
Distance from peak center (kbp)
F
H187 H3K27ac ChIP
NKX2-1 reduced binding sites
Parental
NT sg1
SOX1 sg2
SOX1 sg3
Average Profile
Relative Distance from the Center (bp)
NKX2-1 non-reduced binding sites
Average Profiles around the Center of Sites

Figure 7

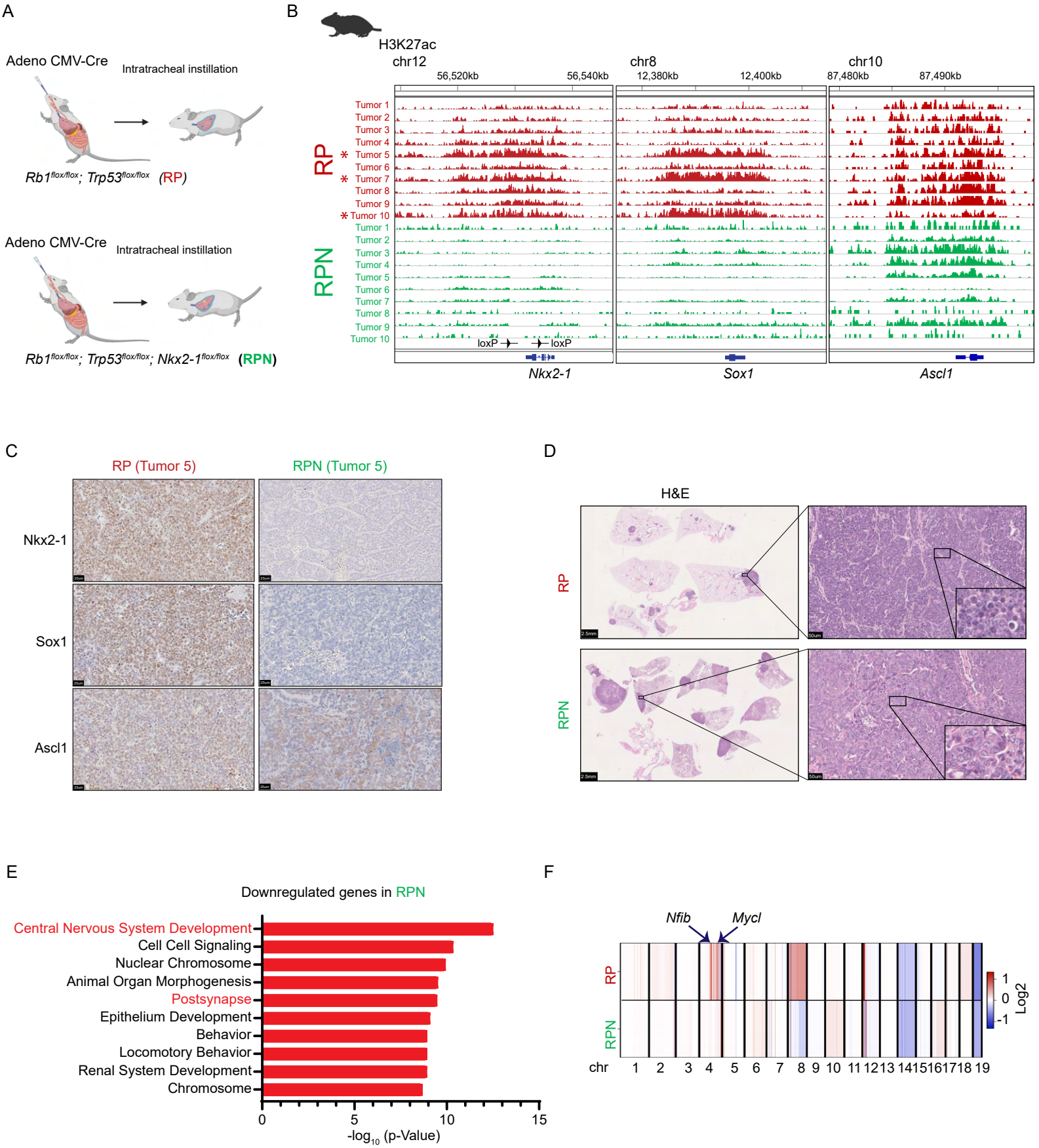
A
Adeno CMV-Cre
Intratracheal instillation
Rb1flox/flox; Trp53flox/flox (RP)
Adeno CMV-Cre
Intratracheal instillation
Rb1flox/flox; Trp53flox/flox; Nkx2-1flox/flox (RPN)
B
H3K27ac
chr12
56,520kb
56,540kb
chr8
12,380kb
12,400kb
chr10
87,480kb
87,490kb
RP
Tumor 1
Tumor 2
Tumor 3
Tumor 4
Tumor 5
Tumor 6
Tumor 7
Tumor 8
Tumor 9
Tumor 10
RPN
Tumor 1
Tumor 2
Tumor 3
Tumor 4
Tumor 5
Tumor 6
Tumor 7
Tumor 8
Tumor 9
Tumor 10
loxP
loxP
Nkx2-1
Sox1
Ascl1
C
RP (Tumor 5)
RPN (Tumor 5)
Nkx2-1
Sox1
Ascl1
D
H&E
RP
RPN
E
Downregulated genes in RPN
Central Nervous System Development
Cell Cell Signaling
Nuclear Chromosome
Animal Organ Morphogenesis
Postsynapse
Epithelium Development
Behavior
Locomotory Behavior
Renal System Development
Chromosome
0
5
10
15
-log10 (p-Value)
F
Nfib
Mycl
RP
RPN
chr
1 2 3 4 5 6 7 8 9 10 11 12 13 14 15 16 17 18 19
1
0
-1
Log2